



# CHORUS

This is the accepted manuscript made available via CHORUS. The article has been published as:

## Effects of biaxial strain on the improper multiferroicity in h-LuFeO<sub>3</sub> films studied using the restrained thermal expansion method

Kishan Sinha, Yubo Zhang, Xuanyuan Jiang, Hongwei Wang, Xiao Wang, Xiaozhe Zhang, Philip J. Ryan, Jong-Woo Kim, John Bowlan, Dmitry A. Yarotski, Yuelin Li, Anthony D.

DiChiara, Xuemei Cheng, Xifan Wu, and Xiaoshan Xu

Phys. Rev. B **95**, 094110 — Published 14 March 2017

DOI: [10.1103/PhysRevB.95.094110](https://doi.org/10.1103/PhysRevB.95.094110)

# Effects of biaxial strain on the improper multiferroicity in h-LuFeO<sub>3</sub> films studied using the restrained thermal expansion method

Kishan Sinha<sup>1</sup>, Yubo Zhang<sup>2</sup>, Xuanyuan Jiang<sup>1</sup>, Hongwei Wang<sup>2</sup>, Xiao Wang<sup>3</sup>, Xiaozhe Zhang<sup>1,4</sup>, Philip J. Ryan<sup>5</sup>, Jong-Woo Kim<sup>5</sup>, John Bowlan<sup>6</sup>, Dmitry A Yarotski<sup>6</sup>, Yuelin Li<sup>5</sup>, Anthony D. DiChiara<sup>5</sup>, Xuemei Cheng<sup>3</sup>, Xifan Wu<sup>2\*†</sup>, Xiaoshan Xu<sup>1,7\*‡</sup>

<sup>1</sup>*Department of Physics and Astronomy, University of Nebraska, Lincoln, Nebraska 68588, USA,*

<sup>2</sup>*Department of Physics, Temple University, Philadelphia, Pennsylvania 19122, USA*

<sup>3</sup>*Department of Physics, Bryn Mawr College, Bryn Mawr, Pennsylvania 19010, USA*

<sup>4</sup>*Department of Physics, Xi'an Jiaotong University, Xi'an 710049, China*

<sup>5</sup>*Advanced Photon Source, Argonne National Laboratory, Argonne, Illinois 60439, USA*

<sup>6</sup>*Center for Integrated Nanotechnologies, Los Alamos National Laboratory, Los Alamos, New Mexico 87545, USA*

<sup>7</sup>*Nebraska Center for Materials and Nanoscience, University of Nebraska, Lincoln, Nebraska 68588, USA*

\*To whom all correspondence should be addressed.

† [xifanwu@temple.edu](mailto:xifanwu@temple.edu); ‡ [xiaoshan.xu@unl.edu](mailto:xiaoshan.xu@unl.edu)

## Abstract

Elastic strain is potentially an important approach in tuning the properties of the improperly multiferroic hexagonal ferrites, the details of which have however been elusive due to the experimental difficulties. Employing the method of restrained thermal expansion, we have studied the effect of isothermal biaxial strain in the basal plane of h-LuFeO<sub>3</sub> (001) films. The results indicate that a compressive biaxial strain significantly enhances the K<sub>3</sub> structural distortion (the order parameter of the improper ferroelectricity), and the effect is larger at higher temperatures. The compressive biaxial strain and the enhanced K<sub>3</sub> structural distortion together, cause an increase in the electric polarization and a reduction in the canting of the weak ferromagnetic moments in h-LuFeO<sub>3</sub>, according to our first principle calculations. These findings are important for understanding the strain effect as well as the coupling between the lattice and the improper multiferroicity in h-LuFeO<sub>3</sub>. The experimental elucidation of the strain effect in h-LuFeO<sub>3</sub> films also suggests that the restrained thermal expansion can be a viable method to unravel the strain effect in many other thin film materials.

How to elastically strain a crystalline material? Conceptionally, the simplest method is to apply high pressure (stress)<sup>1</sup>. Another method, called epitaxial strain, is to grow thin film materials epitaxially on substrates of different lattice constants.<sup>2,3</sup> Here we employ a different method, called the restrained thermal expansion, in which the strain is generated in a film sample by heating the film with a laser pulse that cannot be absorbed by the substrate. Normally, thermal strain can be generated in a material in all crystalline dimensions in an isobaric thermal expansion. In contrast, for a thin film on a substrate, if the film is heated and the substrate remains the same temperature, the out-of-plane dimension of the film is free to expand while the in-plane dimensions of the film can be restrained by the substrate (restrained thermal expansion) [Fig. 1(a)]. By comparing the material properties in the isobaric and restrained thermal expansions, the effect of isothermal compressive strain at a higher temperature can be obtained [Fig. 1(b)] (see S1 in the supplementary materials<sup>4</sup>). This method may generate sizable strain which is difficult in brittle materials for the high-pressure method. It may also avoid side effects in the epitaxial-strain method introduced by the subtle atomic structures at the film/substrate interface.<sup>5</sup>

To demonstrate the method of restrained thermal expansion, we studied the strain effect using this method in hexagonal LuFeO<sub>3</sub> (h-LuFeO<sub>3</sub>), a material that exhibits interesting improperly ferroelectricity and weakly ferromagnetism but very difficult to strain elastically. In an improperly ferroelectric material, the ferroelectric order can be induced by a structural distortion<sup>6</sup>, while in a weakly ferromagnetic material, the ferromagnetic order is typically caused by a structural distortion<sup>7</sup>. Therefore, in materials that are both improperly ferroelectric and weakly ferromagnetic, the structural distortions can play a critical role both in originating the ferroic orders and in coupling them. As a prototypical improper ferroelectric material, h-LuFeO<sub>3</sub> exhibits ferroelectricity below 1050 K and weak ferromagnetism below 130 K.<sup>8-10</sup> The ferroelectricity is induced by a structural distortion [K<sub>3</sub> structural distortion, see Fig. 1(c)].<sup>10-13</sup> The ferromagnetic order, which is parasitic to the antiferromagnetic order, is induced by the K<sub>3</sub> structural distortion both in terms of the creation of the local magnetic moments by the Dzyaloshinskii-Moriya (DM) interactions<sup>14,15</sup> and in terms of the non-zero inter-layer exchange interactions due to the reduction of

symmetry.<sup>10,11,16,17</sup> First principle calculations predict a possible reversal of magnetization by an electric field along the  $c$  axis<sup>11</sup>, and anomalously large magnetoelectric effects in the  $a$ - $b$  plane in h-LuFeO<sub>3</sub><sup>18</sup>, both of which are mediated by the lattice.

In principle, detailed roles of the K<sub>3</sub> structural distortion could be studied by varying the distortion, e.g., by applying an elastic strain. Elastic strain is a promising tool for studying and tuning material properties, such as ferroelectricity, magnetism, catalysis, and transport properties<sup>3,5,19-21</sup>, in addition to the methods such as chemical strain or altering the material structures, owing to the universal coupling between the crystal structure and electronic structures in materials<sup>1,22</sup>. This is unfortunately difficult for h-LuFeO<sub>3</sub>, which is unstable in bulk but can be stabilized in epitaxial thin films: The lack of structurally compatible substrates makes the growth of defect-free films impossible and makes the epitaxial strain difficult to control<sup>9,10,23,24</sup> and there are no bulk counterparts to compare with since the stand-alone hexagonal phase of LuFeO<sub>3</sub> is unstable. As a result, investigations on the strain effect in h-LuFeO<sub>3</sub> have been rare.

Using the method of restrained thermal expansion, we studied the strain effect on the K<sub>3</sub> structural distortion in h-LuFeO<sub>3</sub> films. Here the strain in the film is generated by a laser pulse; the strain and the structural distortion were measured using time-resolved X-ray diffractions. Experimentally, we observed that the compressive biaxial strain in the basal plane of h-LuFeO<sub>3</sub> significantly enhances the K<sub>3</sub> structural distortion, which agrees with the results of our first principle calculation. We also found from our first principle calculations that the compressive strain combined with the enhanced K<sub>3</sub> structural distortion, increases the spontaneous electric polarizations but reduces the weak ferromagnetic moments.

Hexagonal LuFeO<sub>3</sub> (001) thin films (25 nm) were grown using pulsed laser deposition on Al<sub>2</sub>O<sub>3</sub> (001) substrates.<sup>9,16,25</sup> In the restrained thermal expansion, the thermal strains were measured in a laser-pump X-ray-probe style<sup>26-29</sup>, as shown in Fig. 1(d) (see S2 in the supplementary materials<sup>4</sup>). Short durations of restrained thermal expansion in the h-LuFeO<sub>3</sub> thin film, were generated using laser pulses (30 ps, 1 kHz)

with the photon energy (3.2 eV) between the band gap of the  $\text{Al}_2\text{O}_3$  substrate (8.8 eV)<sup>30,31</sup> and that of the h-LuFeO<sub>3</sub> film (2.0 eV)<sup>25,32</sup>. Time resolved diffractions were carried out on h-LuFeO<sub>3</sub> (106) peaks to measure the lattice constants and the structural distortions, using X-ray pulses (80 ps, 12 keV), at different time delay ( $\Delta t$ ) with respect to the laser pulses, with a two-dimensional detector. The temperature dependent X-ray diffractions were carried out to measure the isobaric thermal expansion between 20 and 485 K at the beamline 6-ID-B, and the time-resolved X-ray diffractions were carried out at the beamline 14-ID-B of the Advanced Photon Source at the Argonne National Laboratory. Our first-principles calculations are carried based on density functional theory as implemented in the Vienna ab initio simulation package (VASP)<sup>33</sup>. We adopt the Perdew-Burke-Ernzerhof functional revised for solid (PBEsol)<sup>34</sup> where the spin-polarized generalized gradient approximation (GGA) is made in treating the exchange correlation of the electrons. A cutoff energy of 500 eV is used in the plane-wave basis with a  $4 \times 4 \times 2$  k-point mesh centered at Gamma point. For transition metals, we choose  $U=4.5$  eV and  $J_{\text{H}}=0.95$  eV. The criterion of residual Hellman-Feynman forces for structural relaxation is 0.001 eV/Å.

First, we demonstrate that the thermal strain only occurs in the out of plane direction in the restrained thermal expansion. Figure 2(a) shows the scans of the (106) peak before ( $\Delta t < 0$ ) and after the laser pulse ( $\Delta t = 0.2$  ns) of a  $1.0 \text{ mJ/mm}^2$  fluence. The lattice of the h-LuFeO<sub>3</sub> film at room temperature (without the laser illumination) is used as the reference coordinate system. A clear shift of the diffraction profiles in the reciprocal index  $L$  is observed in Fig. 2(a), indicating a thermal strain along the  $c$  axis. In contrast, there is no observable strain along the  $a$  axis [Fig. 2(b)], suggesting that the in-plane axis is restrained by the  $\text{Al}_2\text{O}_3$  substrate that has no thermal strain because its band gap is too high to absorb the laser photon.

The change of the  $K_3$  structural distortion can be estimated from the intensity change of the (10 $L$ ) peaks, because the  $K_3$  structural distortion is related to the diffraction intensity of (10 $L$ ) peaks as  $I_{(10L)} \propto Q_{K_3}^2$ <sup>9</sup> as a first order approximation if the contribution of the oxygen is ignored (see S3 in the supplementary materials<sup>4</sup>), where  $Q_{K_3}$  is the amplitude of the  $K_3$  structural distortion. As shown in Fig. 2(b), the (106)

peak intensity decreases as the laser pulse heats the film, which is expected, because the (10L) peak vanishes at the ferroelectric  $\rightarrow$  paraelectric transition at high temperature.<sup>9</sup>

Next, we show that the observed time evolution of the thermal strain and the diffraction peak intensity can be explained in terms of thermal conduction. As shown in Fig. 2(b), both the change of peak intensity and the thermal strain decay over time with a similar trend. In the case of thermal conduction, the temperature in the film follows the diffusion equation  $\rho c_M \left( \frac{\partial T}{\partial t} \right)_z = \sigma \left( \frac{\partial^2 T}{\partial z^2} \right)_t$ , where  $\rho$ ,  $c_M$ ,  $T$ ,  $t$ ,  $z$ , and  $\sigma$  are the mass density, the mass specific heat, temperature, time, direction of the thermal conduction, and thermal conductivity respectively.<sup>26,35</sup> At the film/substrate interface, the diffusion equation becomes  $\rho c_M \left( \frac{\partial T}{\partial t} \right)_z = g \Delta T$ , where  $g$  and  $\Delta T$  are the interfacial thermal conductivity and the temperature difference at the interface respectively. The thermal strain  $\frac{\Delta c}{c}$  is expected to decay in a similar trend. The only unknown parameter here is the interfacial thermal conductivity  $g$ . As shown in Fig. 2(b), we fit the time dependence of the thermal strain  $\frac{\Delta c}{c}$  with the diffusion equations using  $g$  as the fitting parameter. The result shows  $g = 3.8 \times 10^8 \text{ W}/(\text{K m}^2)$ , which falls into the proper range of the thermal conductivity of the epitaxial interfaces.<sup>36,37</sup> The fact that the decay of thermal strain can be explained in the light of thermal conduction, suggests that temperature is a well-defined state function during the decay process (see S4 in the supplementary materials<sup>4</sup>).

Because temperature is well defined in the decay process, one may calculate the isothermal strain effect by comparing the properties in the isobaric and restrained thermal expansions at the same temperature [Fig. 1(b)]. The thermal strain in the isobaric thermal expansion, is displayed in Fig. 2(c). As the temperature increases, both  $a$  and  $c$  axes expand. The linear thermal expansion coefficients of the h-LuFeO<sub>3</sub> film around room temperature in both  $a$  and  $c$  directions are found to be  $(8.0 \pm 0.1) \times 10^{-6}$  (see discussion in S5 in the supplementary materials<sup>4</sup>). The intensity of the (106) peak also decreases as the temperature increases [Fig. 2(c)] in the isobaric thermal expansion, as it does in the restrained thermal

expansion. The relation between the (106) peak intensity and the thermal strain  $\frac{\Delta c}{c}$  in the restrained thermal expansion differs obviously from that of the isobaric thermal expansions, as shown in Fig. 2(d), indicating a significant strain effect.

Using the thermal and optical properties of h-LuFeO<sub>3</sub>,<sup>25,32,38</sup> we estimated that the temperature change of the h-LuFeO<sub>3</sub> film after absorbing a 1.0 mJ/mm<sup>2</sup> photon pulse to be  $\sim 460$  K ( $\pm 10\%$ ) (see S6 in the supplementary materials<sup>4</sup>). The relation between the thermal strain  $\frac{\Delta c}{c}$  and the fluence in Fig. 2(b) inset, can be converted to the relation between  $\frac{\Delta c}{c}$  and temperature, which is used to estimate the temperature in the restrained thermal expansion. In Fig. 3(a),  $Q_{K3}$  in the restrained thermal expansion, is calculated according to  $I_{(10L)} \propto Q_{K3}^2$  and the Debye-Waller factors (see S3 in the supplementary materials<sup>4,39</sup>), and plotted against the temperature. Also plotted is the temperature dependence of  $Q_{K3}$  in the isobaric thermal expansion calculated according to the data in Fig. 2(c). Obviously,  $Q_{K3}$  is enhanced in the restrained thermal expansion.

In order to find the effect of isothermal strain on another physical property (e.g. amplitude of K<sub>3</sub> structural distortion  $Q_{K3}$ ), one needs to compare the temperature dependences of the physical property in the isobaric and restrained thermal expansions, as depicted in Fig. 1(b). In the restrained thermal expansion, the change of a general physical property (state function)  $f$ , relative to an initial state  $(a_0, T_0, f_0)$ , can be

written as  $f_a - f_0 \approx \left(\frac{\partial f}{\partial T}\right)_{a, \sigma_c} \Delta T$ , where  $\sigma_c$  is the stress along the  $c$  axis. In the isobaric thermal expansion,

the change of the physical properties corresponds to  $f_P - f_0 \approx \left(\frac{\partial f}{\partial T}\right)_{\sigma_a, \sigma_c} \Delta T$ . The two processes can be

related using Legendre transformation and chain rules of partial differential<sup>35</sup>:

$\left(\frac{\partial f}{\partial T}\right)_{\sigma_a, \sigma_c} = \left(\frac{\partial f}{\partial T}\right)_{a, \sigma_c} + \left(\frac{\partial f}{\partial a}\right)_{T, \sigma_c} \left(\frac{\partial a}{\partial T}\right)_{\sigma_a, \sigma_c}$ , where  $\left(\frac{\partial f}{\partial a}\right)_{T, \sigma_c}$  describes the isothermal strain effect, which can

be found as  $\left(\frac{\partial f}{\partial a}\right)_{\sigma_c, T} \approx -\frac{f_a - f_P}{\Delta T} \frac{1}{\left(\frac{\partial a}{\partial T}\right)_{\sigma_a, \sigma_c}}$ . As shown in Fig. 1(b), if the state after the isobaric thermal



expansion is used as the reference, the strain can be defined as  $\frac{\Delta a}{a} \equiv -\frac{1}{a} \Delta T \left( \frac{\partial a}{\partial T} \right)_{\sigma_a, \sigma_c}$  (compressive); the change of  $f$  caused by the strain is  $f_a - f_p$ . Figure 3(b) shows the relation between  $Q_{K_3,a} - Q_{K_3,p}$  and the in-plane biaxial strain  $\frac{\Delta a}{a}$ . The data points indicate the strain effect at certain temperature (top axis), measured at a certain magnitude of the strain (bottom axis). Obviously, the isothermal compressive biaxial strain enhances the  $K_3$  lattice distortion. In addition, the effect of strain on  $Q_{K_3}$  appears to be larger at higher temperatures.

To better understand the effect of strain on the  $K_3$  structural distortion experimentally measured by the method of restrained thermal expansion, we carried out first-principles calculations based on density functional theory to elucidate the structural distortions at the atomic level. The structures are fully relaxed, for h-LuFeO<sub>3</sub> of the space group symmetry  $P_{63}cm$  under the epitaxial strains ranging from -2% to 2%. Based on the relaxed structures, the mode decompositions were performed using the group theory. The resulting  $Q_{K_3}$  are presented in Fig. 3(c) as a function of biaxial strain. Indeed, our theoretical calculations show that  $Q_{K_3}$  is enhanced (reduced) by the applied compressive (tensile) epitaxial strains, which is consistent with the experimental observation. Under the compressive strain, all the atoms are forced to be more compactly packed within the unit cell. As a result, the intralayer Fe-O bond lengths are slightly reduced and those between Fe and apical oxygen atoms are slightly increased. In addition, the Fe-O bonds within the trimer structure also respond by a buckling behavior compatible with the  $K_3$  structural distortion. As schematically shown in Fig. 1(c), the oxygen atom at the center of the trimer which is shared by three bi-pyramids is moving up, while the other oxygen atoms in the bases of the three bi-pyramids are all moving downwards. As a result,  $Q_{K_3}$  is increased. At the same time, the intralayer distances between two neighboring Fe or Lu atoms are reduced due to the compressive strain.

It is well known that the electric polarization is strongly coupled to the epitaxial strain in properly ferroelectric materials such as BaTiO<sub>3</sub>. Yet, the coupling between the epitaxial strain and functional

properties in multiferroic materials has been much less addressed. We next focus on the tunabilities of functional properties in h-LuFeO<sub>3</sub>, including electric polarization and weak ferromagnetism, under the epitaxial strains. As an improperly multiferroic material, similar to YMnO<sub>3</sub><sup>13</sup>, the ferroelectric distortion in h-LuFeO<sub>3</sub> is driven improperly by the K<sub>3</sub> structural distortion that can be described by the rotation of FeO<sub>5</sub> trigonal bi-pyramids and the buckling of Lu layers [Fig. 1(c)], which is a highly unstable structural instability in its centrosymmetric P<sub>63</sub>/mmc phase.<sup>10-13</sup> Therefore, it is expected that the polarization should increase as  $Q_{K3}$  increases.<sup>12</sup> Indeed, as shown in Fig. 3(d), the polarization is enhanced linearly under the compressive biaxial strain. The change of polarization has a similar rate to that of  $Q_{K3}$ . The tunability of polarization by epitaxial strain is much less than that of the conventional ferroelectric materials such BaTiO<sub>3</sub>. It indicates that the piezoelectricity is relatively small which is consistent with recent experiment in improper hexagonal YMnO<sub>3</sub><sup>40</sup>. The weak ferromagnetism originates from both the DM interaction and single ion anisotropy. The magnitude of the DM interaction depends on the DM vector  $\mathbf{D} \sim |\mathbf{r}_{\text{Fe-Fe}} \times \boldsymbol{\delta}_z|$ <sup>11,14,15</sup>, where  $\mathbf{r}_{\text{Fe-Fe}}$  is the displacement vector between the two iron atoms and  $\boldsymbol{\delta}_z$  is the displacement vector along [001] direction for the oxygen atom shared by three bi-pyramids in the trimer shown in Fig. 1(c) respectively. Since  $\boldsymbol{\delta}_z$  is closely associated with the trimerization measured by the  $Q_{K3}$ , the weak ferromagnetism was found to be intrinsically related to the K<sub>3</sub> structural distortion. Therefore, an enhanced ferromagnetic moment is expected at a larger  $Q_{K3}$  under compressive strain. However, the compressive strain also brings the two Fe atom closer which reduces the displacement vector  $\mathbf{r}_{\text{Fe-Fe}}$  more rapidly [see Fig. 1(c)]; this actually reduces amplitude of cross product of the DM vector. As a result, the canting ferromagnetic moment is rather decreased under compressive biaxial strain [see Fig. 3(d)].

In conclusion, we have demonstrated the restrained thermal expansion method by elucidating the effect of biaxial strain on the structural distortion in improperly multiferroic h-LuFeO<sub>3</sub>. We have found a significant coupling between the biaxial strain in the basal plane and the K<sub>3</sub> structural distortion in h-LuFeO<sub>3</sub>, which in turn couples to the electric and magnetic polarizations in this improperly ferroelectric and weakly ferromagnetic material. In particular, the compressive strain enhances the K<sub>3</sub> structural

distortion and the ferroelectric polarization, but reduces the canting of weak ferromagnetic moments. The elucidation of the strain effect in h-LuFeO<sub>3</sub> is an important advancement of our understanding on the coupling between the lattice and the improper multiferroicity. It is essential to the recently demonstrated hexagonal-ferrite super-lattice structures that are promising for room-temperature multiferroicity<sup>41</sup>, since the structural distortions in the h-LuFeO<sub>3</sub> layers are responsible for the ferroelectricity. The experimental characterization of strain effect in h-LuFeO<sub>3</sub>, can potentially be extended to measure the electronic and magnetic properties, when additional probes (e.g. optical or soft X-ray) are included. This could be especially important for studying the epitaxial thin films for which the strain effects haven't been fully investigated due to the imperfection in epitaxy or the lack of bulk counterparts.

## Acknowledgement

The experimental effort in this work was mainly supported by the National Science Foundation (NSF), DMR under Award DMR-1454618. X.M.C. acknowledges partial support from National Science Foundation Grant No. DMR-1053854. The theoretical effort was supported by the Air Force Office of Scientific Research under FA9550-13-1-0124. This research used resources of the Advanced Photon Source, a U.S. Department of Energy (DOE) Office of Science User Facility operated for the DOE Office of Science by Argonne National Laboratory under Contract No. DE-AC02-06CH11357. Use of BioCARS was also supported by the National Institute of General Medical Sciences of the National Institutes of Health under grant number R24GM111072. The content is solely the responsibility of the authors and does not necessarily represent the official views of the National Institutes of Health. Time-resolved set-up at Sector 14 was funded in part through a collaboration with Philip Anfinrud (NIH/NIDDK).

## References

- <sup>1</sup> M. Hanfland, K. Syassen, N.E. Christensen, and D.L. Novikov, *Nature* **408**, 174 (2000).
- <sup>2</sup> D.G. Schlom, L.-Q. Chen, C.J. Fennie, V. Gopalan, D.A. Muller, X. Pan, R. Ramesh, and R. Uecker, *MRS Bull.* **39**, 118 (2014).
- <sup>3</sup> D.G. Schlom, L.-Q. Chen, C.-B. Eom, K.M. Rabe, S.K. Streiffer, and J.-M. Triscone, *Annu. Rev. Mater. Res* **37**, 589 (2007).
- <sup>4</sup> See Supplemental Material at [url] for more details in the experimental method, data analysis, and the discussion of the thermodynamic processes.
- <sup>5</sup> H. Wang, J. Wen, D.J. Miller, Q. Zhou, M. Chen, H.N. Lee, K.M. Rabe, and X. Wu, *Phys. Rev. X* **6**, 11027 (2016).
- <sup>6</sup> A.P. Levanyuk and D.G. Sannikov, *Sov. Phys. Uspekhi* **17**, 199 (1974).
- <sup>7</sup> R.L. White, *J. Appl. Phys.* **40**, 1061 (1969).
- <sup>8</sup> Y.K. Jeong, J. Lee, S. Ahn, S.-W. Song, H.M. Jang, H. Choi, and J.F. Scott, *J. Am. Chem. Soc.* **134**, 1450 (2012).
- <sup>9</sup> W. Wang, J. Zhao, W. Wang, Z. Gai, N. Balke, M. Chi, H.N. Lee, W. Tian, L. Zhu, X. Cheng, D.J. Keavney, J. Yi, T.Z. Ward, P.C. Snijders, H.M. Christen, W. Wu, J. Shen, and X. Xu, *Phys. Rev. Lett.* **110**, 237601 (2013).
- <sup>10</sup> X. Xu and W. Wang, *Mod. Phys. Lett. B* **28**, 1430008 (2014).
- <sup>11</sup> H. Das, A.L. Wysocki, Y. Geng, W. Wu, and C.J. Fennie, *Nat Commun* **5**, 2998 (2014).
- <sup>12</sup> C. Xu, Y. Yang, S. Wang, W. Duan, B. Gu, and L. Bellaiche, *Phys. Rev. B* **89**, 205122 (2014).
- <sup>13</sup> C.J. Fennie and K.M. Rabe, *Phys. Rev. B* **72**, 100103 (2005).
- <sup>14</sup> I. Dzyaloshinsky, *J. Phys. Chem. Solids* **4**, 241 (1958).

- <sup>15</sup> T. Moriya, Phys. Rev. **120**, 91 (1960).
- <sup>16</sup> S. Cao, X. Zhang, T.R. Paudel, K. Sinha, X. Wang, X. Jiang, W. Wang, S. Brutsche, J. Wang, P.J. Ryan, J.-W. Kim, X. Cheng, E.Y. Tsymbal, P.A. Dowben, and X. Xu, J. Phys. Condens. Matter **28**, 156001 (2016).
- <sup>17</sup> H. Wang, I. V. Solovyev, W. Wang, X. Wang, P.P.J. Ryan, D.J. Keavney, J.-W. Kim, T.Z. Ward, L. Zhu, J. Shen, X.M. Cheng, L. He, X. Xu, X. Wu, J. Shen, L. He, X. Xu, and X. Wu, Phys. Rev. B **90**, 14436 (2014).
- <sup>18</sup> M. Ye and D. Vanderbilt, Phys. Rev. B **92**, 35107 (2015).
- <sup>19</sup> J. Welsch, J.L. Hoyt, and J.F. Gibbons, IEEE Electron Device Lett. **15**, 100 (1994).
- <sup>20</sup> S.W. Bedell, A. Khakifirooz, and D.K. Sadana, MRS Bull. **39**, 131 (2014).
- <sup>21</sup> B. Yildiz, MRS Bull. **39**, 147 (2014).
- <sup>22</sup> D. Yu, J. Feng, and J. Hone, MRS Bull. **39**, 157 (2014).
- <sup>23</sup> E. Magome, C. Moriyoshi, Y. Kuroiwa, A. Masuno, and H. Inoue, Jpn. J. Appl. Phys. **49**, 09ME06 (2010).
- <sup>24</sup> J.A. Moyer, R. Misra, J.A. Mundy, C.M. Brooks, J.T. Heron, D.A. Muller, D.G. Schlom, and P. Schiffer, APL Mater. **2**, 12106 (2014).
- <sup>25</sup> W. Wang, H. Wang, X. Xu, L. Zhu, L. He, E. Wills, X. Cheng, D.J. Keavney, J. Shen, X. Wu, and X. Xu, Appl. Phys. Lett. **101**, 241907 (2012).
- <sup>26</sup> H. Wen, P. Chen, M.P. Cosgriff, D.A. Walko, J.H. Lee, C. Adamo, R.D. Schaller, J.F. Ihlefeld, E.M. Dufresne, D.G. Schlom, P.G. Evans, J.W. Freeland, and Y. Li, Phys. Rev. Lett. **110**, 37601 (2013).
- <sup>27</sup> D. Daranciang, M.J. Highland, H. Wen, S.M. Young, N.C. Brandt, H.Y. Hwang, M. Vattilana, M. Nicoul, F. Quirin, J. Goodfellow, T. Qi, I. Grinberg, D.M. Fritz, M. Cammarata, D. Zhu, H.T. Lemke,

- D.A. Walko, E.M. Dufresne, Y. Li, J. Larsson, D.A. Reis, K. Sokolowski-Tinten, K.A. Nelson, A.M. Rappe, P.H. Fuoss, G.B. Stephenson, and A.M. Lindenberg, *Phys. Rev. Lett.* **108**, 87601 (2012).
- <sup>28</sup> Y. Li, R.D. Schaller, M. Zhu, D.A. Walko, J. Kim, X. Ke, L. Miao, and Z.Q. Mao, *Sci. Rep.* **6**, 19302 (2016).
- <sup>29</sup> Y. Li, C. Adamo, P. Chen, P.G. Evans, S.M. Nakhmanson, W. Parker, C.E. Rowland, R.D. Schaller, D.G. Schlom, D. a Walko, H. Wen, and Q. Zhang, *Sci. Rep.* **5**, 16650 (2015).
- <sup>30</sup> R.H. French, *J. Am. Ceram. Soc.* **73**, 477 (1990).
- <sup>31</sup> E.O. Filatova and A.S. Konashuk, *J. Phys. Chem. C* **119**, 20755 (2015).
- <sup>32</sup> B.S. Holinsworth, D. Mazumdar, C.M. Brooks, J.A. Mundy, H. Das, J.G. Cherian, S.A. McGill, C.J. Fennie, D.G. Schlom, and J.L. Musfeldt, *Appl. Phys. Lett.* **106**, 82902 (2015).
- <sup>33</sup> G. Kresse and J. Furthmüller, *Phys. Rev. B* **54**, 11169 (1996).
- <sup>34</sup> J. Perdew, A. Ruzsinszky, G. Csonka, O. Vydrov, G. Scuseria, L. Constantin, X. Zhou, and K. Burke, *Phys. Rev. Lett.* **100**, 136406 (2008).
- <sup>35</sup> R.J. Hardy and C. Binek, *Thermodynamics and Statistical Mechanics* □: *An Integrated Approach* (John Wiley & Sons Inc., Chichester, West Sussex, 2014).
- <sup>36</sup> R.M. Costescu, M.A. Wall, and D.G. Cahill, *Phys. Rev. B* **67**, 54302 (2003).
- <sup>37</sup> H.K. Lyeo and D.G. Cahill, *Phys. Rev. B* **73**, 144301 (2006).
- <sup>38</sup> P.A. Sharma, J.S. Ahn, N. Hur, S. Park, S.B. Kim, S. Lee, J.G. Park, S. Guha, and S.W. Cheong, *Phys. Rev. Lett.* **93**, 177202 (2004).
- <sup>39</sup> L.-M. Peng, G. Ren, S.L. Dudarev, and M.J. Whelan, *Acta Crystallogr. Sect. A* **52**, 456 (1996).
- <sup>40</sup> Y. Geng, H. Das, A.L. Wysocki, X. Wang, S.-W. Cheong, M. Mostovoy, C.J. Fennie, and W. Wu, *Nat. Mater.* **13**, 163 (2014).

<sup>41</sup> J.A. Mundy, C.M. Brooks, M.E. Holtz, J.A. Moyer, H. Das, A.F. Rébola, J.T. Heron, J.D. Clarkson, S.M. Disseler, Z. Liu, A. Farhan, R. Held, R. Hovden, E. Padgett, Q. Mao, H. Paik, R. Misra, L.F. Kourkoutis, E. Arenholz, A. Scholl, J.A. Borchers, W.D. Ratcliff, R. Ramesh, C.J. Fennie, P. Schiffer, D.A. Muller, and D.G. Schlom, *Nature* **537**, 523 (2016).



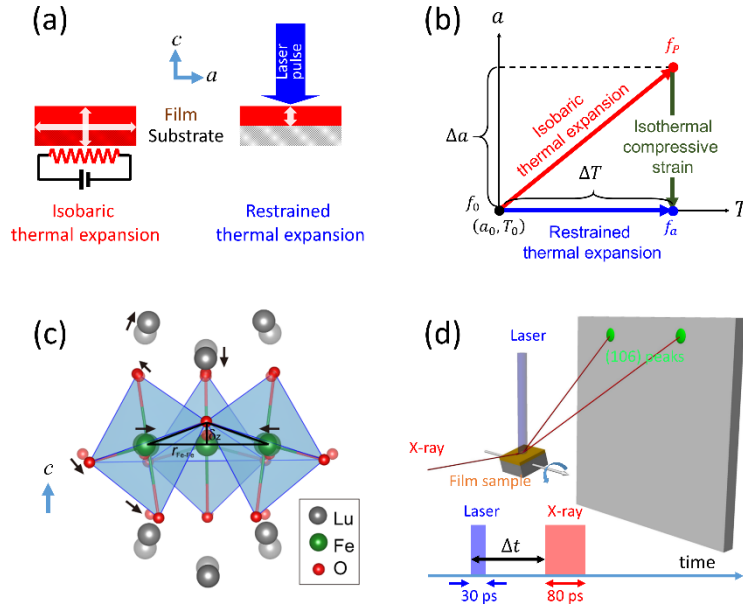


**Figure 1.** (color online) (a) Schematics of the strain generated by the restrained thermal expansion in comparison with that by the isobaric thermal expansion. The arrows indicate the directions of thermal expansion. (b) Illustration of the restrained thermal expansion and isobaric thermal expansion in the  $(a, T)$  space, where  $a$  is the in-plane lattice constants,  $T$  is temperature,  $f$  is a general physical property. (c) Trimer model of the  $K_3$  structural distortion in  $h\text{-LuFeO}_3$ , which corresponds to the rotation of  $\text{FeO}_5$  trigonal bipyramids, the buckling of the Lu layers, and the trimerization. The arrows indicate the atomic displacements when  $K_3$  is enhanced under the compressive biaxial strain. (d) Illustration of the experimental setup for the pump (laser) and probe (x-ray) measurements.

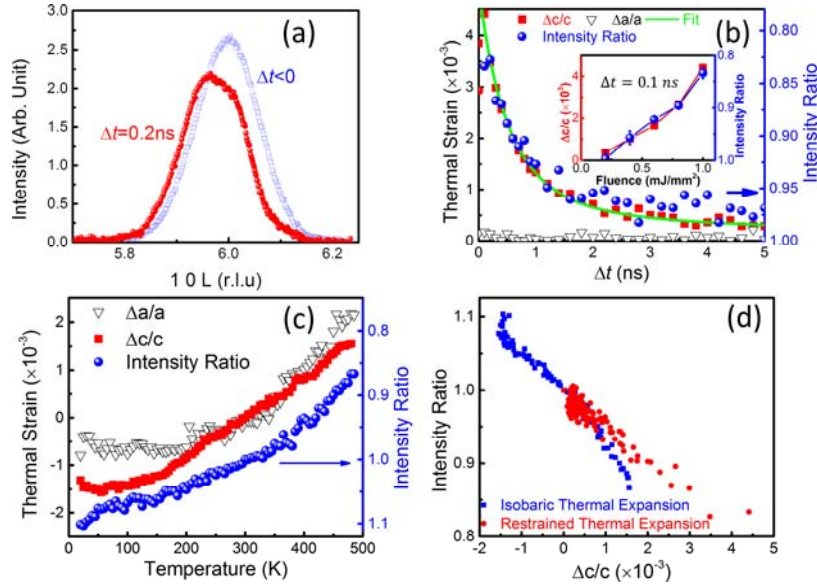


**Figure 2.** (color online) Thermal strain and the intensity change of the (106) peak in the restrained and isobaric thermal expansions. (a) The diffraction profile of the (106) peak before and after the laser ( $1.0 \text{ mJ}/\text{mm}^2$ ) pulse. (b) The decay of the thermal strain  $\frac{\Delta c}{c}$  and the (106) peak intensity in the restrained thermal expansion, as well as the fit using the thermal conduction model. Inset: the thermal strain  $\frac{\Delta c}{c}$  and the (106) peak intensity at  $t_{\text{delay}} = 0.1 \text{ ns}$  as a function of laser fluence. (c) The thermal strain and (106) peak intensity, as a function temperature in the isobaric thermal expansion. (d) The relation between the (106) peak intensity and the thermal strain  $\frac{\Delta c}{c}$  in the restrained and isobaric thermal expansions. The (106) peak intensities are normalized using the values at room temperature.

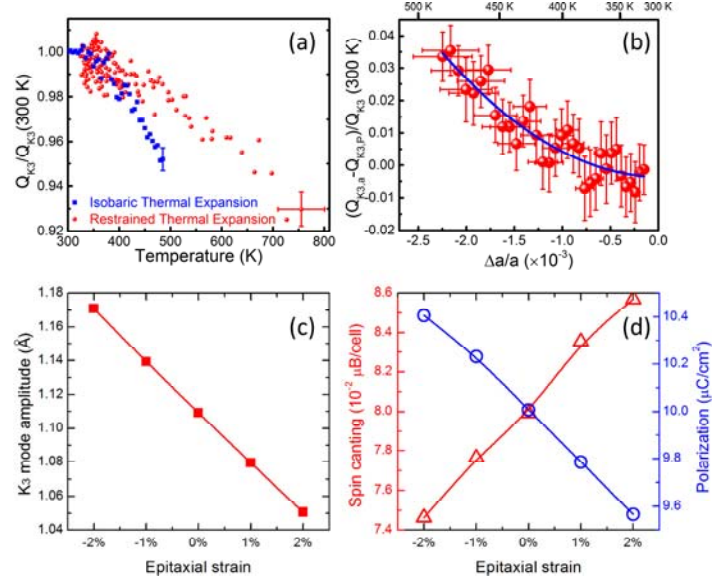


**Figure 3.** (color online) (a) Temperature dependence of the amplitude of the  $K_3$  distortion ( $Q_{K_3}$ ) in both isobaric and restrained thermal expansion as a function of temperature. Representative error bars are displayed. (b) The effect of isothermal biaxial compressive strain on  $Q_{K_3}$ . Each data point represents a change of  $Q_{K_3}$  caused by a strain  $\frac{\Delta a}{a}$  (bottom axis) at the corresponding temperature (top axis). The line is a guide to the eyes. (c) and (d) are the effect of the biaxial strain  $\frac{\Delta a}{a}$  on the  $K_3$  distortion and on the electric polarization and the weak ferromagnetic moment respectively, calculated using the density functional theory.